

**Turbulent mixing and the formation of an intermediate nepheloid layer above the Siberian continental shelf break**

Shultz, Kirsten; Buttner, Stefan; Rogge, Andreas; Janout, M.A.; Holemann, J.; Rippeth, Tom

Geophysical Research Letters

E-pub ahead of print: 26/04/2021

Peer reviewed version

[Cyswllt i'r cyhoeddiad / Link to publication](#)

Dyfyniad o'r fersiwn a gyhoeddwyd / Citation for published version (APA):

Shultz, K., Buttner, S., Rogge, A., Janout, M. A., Holemann, J., & Rippeth, T. (2021). Turbulent mixing and the formation of an intermediate nepheloid layer above the Siberian continental shelf break. *Geophysical Research Letters*, [e2021GL092988]. <http://10.1029/2021GL092988>

Hawliau Cyffredinol / General rights

Copyright and moral rights for the publications made accessible in the public portal are retained by the authors and/or other copyright owners and it is a condition of accessing publications that users recognise and abide by the legal requirements associated with these rights.

- Users may download and print one copy of any publication from the public portal for the purpose of private study or research.
- You may not further distribute the material or use it for any profit-making activity or commercial gain
- You may freely distribute the URL identifying the publication in the public portal ?

Take down policy

If you believe that this document breaches copyright please contact us providing details, and we will remove access to the work immediately and investigate your claim.

Turbulent mixing and the formation of an intermediate nepheloid layer above the Siberian continental shelf break

Kirstin Schulz¹, Stefan Büttner², Andreas Rogge^{1,2}, Markus Janout¹, Jens Hölemann¹, Tom P. Rippeth³

¹Alfred Wegener Institute, Helmholtz Centre for Polar and Marine Research, Bremerhaven, Germany

²Institute for Ecosystem Research, Christian Albrechts University Kiel, Kiel, Germany

³School of Ocean Sciences, Bangor University, Bangor, UK

Key Points:

- First direct observation of an intermediate nepheloid layer in the Eurasian part of the Arctic Ocean
- Coinciding strong midwater turbulence is likely caused by a down-slope current displacing isopycnals
- Similar downslope flow events exhibit a strong seasonality towards the ice free season

Corresponding author: Kirstin Schulz, kirstin.schulz@awi.de

This article has been accepted for publication and undergone full peer review but has not been through the copyediting, typesetting, pagination and proofreading process, which may lead to differences between this version and the [Version of Record](#). Please cite this article as doi: [10.1029/2021GL092988](https://doi.org/10.1029/2021GL092988).

This article is protected by copyright. All rights reserved.

Abstract

Intermediate nepheloid layers (INLs) form important pathways for the cross-slope transport and vertical export of particulate matter, including carbon. While intermediate maxima in particle settling fluxes have been reported in the Eurasian Basin of the Arctic Ocean, direct observations of turbid INLs above the continental slope are still lacking. In this study, we provide the first direct evidence of an INL, coinciding with enhanced mid-water turbulent dissipation rates, over the Laptev Sea continental slope in summer 2018. Current velocity data show a period of enhanced downslope flow with depressed isopycnals, suggesting that the enhanced turbulent dissipation is probably the consequence of the presence of an unsteady lee wave. Similar events occur mostly during ice free periods, suggesting an increasing frequency of episodic cross-slope particle transport in the future. The discovery of the INL and the episodic generation mechanism provide new insights into particle transport dynamics in this rapidly changing environment.

Plain Language Summary

In the Arctic Ocean deep basins, only a tiny fraction of the algae that grows in the surface layer sinks down to the sea floor. Most of the particles reaching the sea floor originate from the shallower regions closer to the coast. These particles have already settled on the sea floor once, and originate from rivers or algae that grew, died and sank down in shallow regions. Later, these particles are lifted off the ground again by strong turbulent motions, and transported towards deeper regions in the middle of the water column. These lift-off and transport events happen only occasionally, and have not been directly observed in the Eurasian part of the Arctic Ocean yet. Also, we present a new mechanism for the creation of turbulence, which is necessary to lift particles off the sea floor. This mechanism happens mostly during the summer season, when less sea ice is present. Based on this seasonality, it is likely that sediment transport events will become more frequent in the future, when the Arctic sea ice is further declining.

1 Introduction

Particle transport pathways and organic carbon cycling in the Arctic Ocean are substantially different compared to the rest of the world's pelagic oceans (Hwang et al., 2008; Honjo et al., 2010). The vertical export of surface primary production particulate organic matter by gravitational sinking and migrating zooplankton is inefficient (Honjo

47 et al., 2010), and only contributes to 1-2% of the interior basin particulate organic car-
48 bon (POC) supply (Hwang et al., 2015). Particle and POC settling fluxes are strongly
49 affected by sea ice melt, via the deposition of large under-ice algae biomass (Boetius et
50 al., 2013), and the release of sediments from dirty sea ice (e.g. Krumpfen et al., 2019).
51 Both processes are episodic in time, and are becoming increasingly important in the cen-
52 tral Arctic Ocean due to intensified melt. In the vicinity of the basin margins, particle
53 fluxes are dominated by lateral advection of resuspended lithogenic ballasted material
54 from the continental slopes (Fahl & Nöthig, 2007; Hwang et al., 2008; Honjo et al., 2010;
55 Hwang et al., 2015; Forest et al., 2015, 2016; Osborne & Forest, 2016; Xiang & Lam, 2020).
56 This principal transport pathway closely links the basin interior and the disproportion-
57 ately large shelf sea areas of the Arctic. Anticipated changes in the near coastal areas
58 – like increased anthropogenic use or thawing permafrost – therefore have the potential
59 to impact the entire Arctic Ocean. Resolving the transport mechanisms connecting the
60 Arctic shelf and interior basin is hence a key issue to understand organic carbon cycling
61 and particle transport pathways (Forest et al., 2015), especially in the light of a rapidly
62 changing Arctic system, which will likely impact particle sources and transport (Xiang
63 & Lam, 2020).

64 Isopycnal intrusions of detached bottom nepheloid layers, forming intermediate neph-
65 eloid layers (INLs), may initiate the basin-ward transport of resuspended particles from
66 the continental margin (Hwang et al., 2008). INLs have been observed in the vicinity of
67 continental margins at lower latitudes (Pak et al., 1980; Puig & Palanques, 1998; Thorpe
68 & White, 1988; Cacchione & Drake, 1986; Azetsu-Scott et al., 1995; De Madron et al.,
69 1990; de Madron et al., 1999; Gardner & Walsh, 1990; van Weering et al., 2001), where
70 the turbid bottom layer is detached from the topographic slope and spreads seaward (McPhee-
71 Shaw et al., 2004). These INLs form important pathways for the transport of particles
72 including carbon, nutrients and lithogenic material from the shelf to the deep ocean (van
73 Weering et al., 2001; McCave & Hall, 2002; McPhee-Shaw et al., 2004), and can thus con-
74 tribute to the long-term sequestration of carbon in the ocean (McPhee-Shaw, 2006), and
75 affect the deep-water benthic population structure (Puig et al., 2001). Most INLs are
76 linked to enhanced turbulent mixing often associated with breaking of an internal tide
77 (Dickson & McCave, 1986; Cacchione & Drake, 1986; Thorpe & White, 1988; Azetsu-
78 Scott et al., 1995; de Madron et al., 1999; McPhee-Shaw et al., 2004). In the Arctic Ocean,
79 however, most continental slope regions are located poleward of the critical latitude for

80 the generation of a freely propagating linear internal tide, but the generation of an un-
81 steady lee-wave can result in significant turbulent mixing (Fer et al., 2015; Rippeth et
82 al., 2017; Fer et al., 2020).

83 The existence of INLs and their importance for seaward particle fluxes in the Am-
84 erasian part of the Arctic Ocean was first suspected by OBrien et al. (2006), over the
85 slope of the Mackenzie shelf in the Canadian Beaufort Sea, and later confirmed by Forest
86 et al. (2007). Strong atmospheric cooling, ice formation and the resulting thermohaline
87 convection provide a mechanism for shelf sediment resuspension and advection at high
88 latitudes, explaining the observed dominant contribution of resuspended material to the
89 vertical POC flux over the Mackenzie shelf slope in fall and winter (Forest et al., 2007).
90 Mesoscale eddies are suspected to further amplify basin-ward transport of turbid waters
91 originating from the shelf and upper slope regions (Forest et al., 2007, 2015; Osborne &
92 Forest, 2016). Furthermore, large scale wind dynamics inducing downwelling (Osborne
93 & Forest, 2016) and resuspension by surges of fast barotropic currents (Forest et al., 2016)
94 were found to facilitate shelf-basin particle transport in the Canadian Beaufort Sea.

95 Observations of INLs in the Eurasian Arctic Ocean are, however, extremely scarce.
96 Fahl and Nöthig (2007) found high vertical fluxes of mostly lithogenic material at inter-
97 mediate depths above the southern Lomonosov Ridge, presumably caused by lateral ad-
98 vection from the Laptev Sea continental margin. Xiang and Lam (2020) report interme-
99 mediate lithogenic particle maxima in the Arctic basins, with elevated concentrations on
100 the Eurasian side of the Lomonosov Ridge, and suspect dense-water cascading in win-
101 ter as the major lateral transport process. Evidence of a turbid INL was observed over
102 the Laptev Sea inner shelf (water depths <60 m), probably caused by a displacement
103 of the bottom nepheloid layer in the vicinity of a shallow bank (Wegner et al., 2003). Even
104 though the Siberian continental slope region is frequently sampled since the early 2000s
105 in the context of the NABOS (Nansen and Amundsen Basins Observational System), and
106 more recently the CATS (The Changing Arctic Transpolar System) project, to the au-
107 thors knowledge no direct observations of turbid INLs have been reported in this region,
108 or anywhere at latitudes polewards of the critical M2-latitude at 74.5°N.

109 Here we provide the first evidence of the presence of intermittent INLs over the con-
110 tinental shelf break of the Laptev Sea. The evidence is based on vertical profiles of par-
111 ticulate matter concentration, size distribution and carbon content, and contemporane-

ous turbulent microstructure measurements, taken during an ice-free period in the summer of 2018. Coincident velocity measurements provide clues as to the episodic generation mechanism and suggest it is seasonal in nature.

2 Data and Methods

From August 18 to September 29, 2018, the continental shelf break region of the Laptev and East Siberian Sea, between between 92°E and 160°E, was sampled during an expedition with the *Akademik Tryoshnikov*. In total, 11 cross-slope transects were performed, distributed over an approximately 2500 km distance along the shelf break. In the following, we will mainly present data from one transect in the central Laptev Sea, at 77°N, 126°E (see Tarasenko et al., 2021; Schulz et al., 2021, and Fig. 1 for details). At each station, ship-based conductivity, temperature, depth (CTD) casts were carried out, along with 2–3 consecutive casts with a microstructure (MSS) profiler, equipped with shear probes to estimate turbulent dissipation rates. Depending on the water depth, one MSS casts took around 10–20 minutes, the 2–3 performed MSS casts were subsequently averaged to obtain one mean profile per station. Both CTD and MSS were equipped with an optical backscatter (OBS) turbidity sensor, which was calibrated with 166 in-situ water filtration samples for total particulate matter (PM) concentration ($\text{PM (mg L}^{-1}\text{)} = 1.88 \times \text{OBS (NTU)} + 0.61$, $R^2=0.82$). For each PM sample, a water volume of 1–2 L was filtered through pre-weighed MILLIPORE filters with a diameter of 47 mm and a pore size of 0.45 μm , and dried for 24 hours at 60°C directly after sampling and again before weighing in the laboratory.

An Underwater Vision Profiler 5hd (Hydroptic, France) was mounted inside the CTD frame to obtain profiles of particle abundances and their size distribution. Sampling frequency of the UVP was 20 Hz, the sampling volume was approximately 1 L. Post-processing of the large particulate matter data and vignettes was accomplished using the ImageJ based software Zooprocess (Gorsky et al., 2010).

In addition, 92 size fractionated POC samples were taken. Fine particles <100 μm (sample volume 1-2 L) were filtered over a 100 μm MILLIPORE nylon mesh and subsequently onto 0.8 μm GFF filters (Whatman), dried and stored at -80°C until acidification in the laboratory to remove carbonates. An element analyzer (Euro EA Elemental Analyser, Model: EURO EA 3000, EUROVECTOR S.p.A., Via Tortona 5, Milano,

Italy) was used to quantify carbon content of the tin encapsulated samples. Excluding fluorescent data points near the surface, POC data was related to turbidity values from the OBS sensor on the CTD. A Theil-Sen regression, which is less sensitive to the many outliers in the data (Sprent, 2012), was used to obtain the linear regression $\text{POC}_{<100\mu\text{m}} (\text{mol L}^{-1}) = 2.62 \times 10^{-6} \times \text{OBS (NTU)} + 6.93 \times 10^{-7}$. POC data for the fraction of large particles $>100 \mu\text{m}$ (the UVP size range, sample volume 20–60 L), exhibited no sufficient correlation to the volumetric particle concentration measured with the UVP. Hence, we only use the particle size distribution data from the UVP, and do not estimate POC content in the large particle fraction. Consequently, POC values in this study refer to POC in particles $<100 \mu\text{m}$, and are likely an underestimation of the total POC content.

Furthermore, a mooring line consisting of an upward-looking 75 kHz ADCP (Workhorse Sentinel, Teledyne RD Instruments), profiling the water column between 40–230 m in 5 m bins at hourly resolution, and three CTDs (SBE37, Sea-Bird Scientific, temporal resolution of 15 minutes) at 49 m, 135 m, and 236 m water depth was deployed on the transect in September 2015, and recovered during the transect measurements. Only data from the lowermost two CTD was used in this study, as the shallowest CTD was affected by tilt on the mooring line in the presence of strong currents. The acoustic backscatter data of the ADCP was not suited to describe PM concentration, we suspect that the majority of suspended particles were too small to reflect the 75 kHz acoustic signal. Details on the instrumentation, data processing and sampling procedures can be found in Schulz et al. (2021) (MSS and CTD) and Polyakov, Rippeth, Fer, Alkire, et al. (2020); Polyakov, Rippeth, Fer, Baumann, et al. (2020) (ADCP).

3 Results

3.1 Particle distribution and turbulent mixing

At station S3, located at approximately 360 m water depth at the Laptev Sea continental slope, we observed an intermediate water layer characterized by unusually high PM concentrations, along with strongly enhanced turbulent dissipation rates over the whole water column (Fig. 1). The integrated PM concentration in this INL (60–310 m) is approximately 650 g m^{-2} , the integrated POC content is 10 g m^{-2} . No comparable turbid and turbulent layer was found on any of the other ten cross-slope transects performed during the expedition. Mid-water turbulent dissipation rates at S3 are up to $10^{-7} \text{ W kg}^{-1}$,

174 two orders of magnitude higher than the values of 10^{-9} W kg $^{-1}$ typically observed in
175 intermediate water layers above the continental slope (based on stations measured at wa-
176 ter depths between 250–600 m on other transect during the same expedition, see Fig.1a,
177 b).

178 Already less than 10 km further offshore, at station S4, no enhanced PM concen-
179 trations or strongly enhanced turbulence at intermediate layers are present. At the two
180 shallower shelf stations on this transect (S1 and S2, Fig. 1), a frictional turbid bottom
181 boundary layer with a vertical extent of 25 m (S1) to 35 m (S2) is found. PM concen-
182 trations there are higher than typically found in the near bottom layer at other shelf sta-
183 tions during the same measurement campaign, but much lower than the mid-water max-
184 imum PM concentration at station S3 (Fig. 2c). This PM distribution points to a source
185 of turbidity further down-slope, between S2 and S3, rather than on the shelf.

186 The INL at S3 is characterized by a potential density anomaly of $\sigma_{\theta} = 27.74$ kg m $^{-3}$,
187 corresponding to the density of the near bottom waters at S2 (Fig. 2a, b). Together with
188 the similar particle size distribution (PSD) observed in both layers (Fig. 2c), at least in
189 the range of particles smaller than 1.29 mm, these similar water mass properties point
190 to a common origin of the encountered high PM concentrations. Again, the total amount
191 of (small) particles encountered in the INL at S3 is on average 3 times higher than in
192 the near bottom layer at S2. The near bottom water properties and PSD at S1, how-
193 ever, differ from those at S2 and S3: The water is colder, less saline and characterized
194 by a lower density of $\sigma_{\theta} = 27.69$ kg m $^{-3}$. Only particles smaller than 0.323 mm exhibit
195 the same size class distribution at S1, compared to S2 and S3. In contrast, large parti-
196 cles exhibit a trend towards higher concentrations at the shallower shelf stations. This
197 station is still some 100 km away from any riverine input, hence the large particles might
198 be locally resuspended (i.e. the bottom sediment composition is different compared to
199 the origin of the INL) or were transport up-slope within the bottom boundary layer (Schulz
200 & Umlauf, 2016; Schulz et al., 2017).

201 **3.2 Flow regime**

202 Current velocities, measured with the ADCP moored at M2, generally exhibit a
203 flow to the east, roughly aligned with the isobaths, and associated with with the Arc-
204 tic Circumpolar Current transporting Atlantic Water along the Arctic Basin margins,

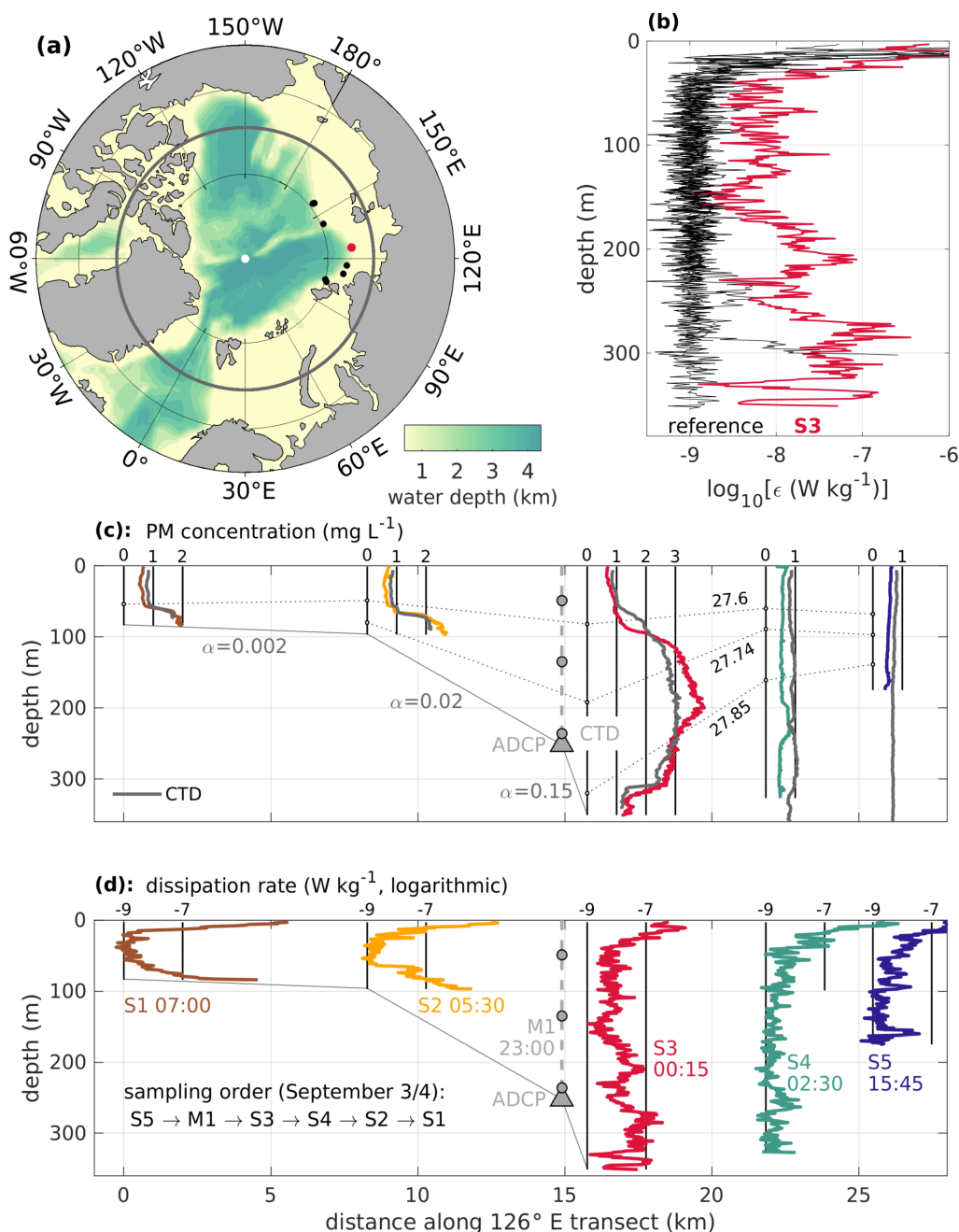


Figure 1. (a) Map of the Arctic Ocean, with the critical M_2 latitude (gray line) and the position of the INL (red dot) and reference stations (black dots) indicated, (b) vertical profiles of turbulent dissipation rate (W kg^{-1}) at station S3 (red) and the reference stations (black). Vertical profiles of (c) PM concentration (mg L^{-1} , measurement position at the vertical 0 line) and (d) turbulent dissipation rate (W kg^{-1} , measurement position at the vertical -9 line), measured along the cross-slope transect at 126°E . In (c), colored lines indicate data from the microstructure profiler, gray lines refer to CTD profiles at the same position, isopycnals are indicated with dotted black lines. The dashed gray line in (c) and (d) indicates the position of the mooring chain with the ADCP (triangle) and CTDs (circles).

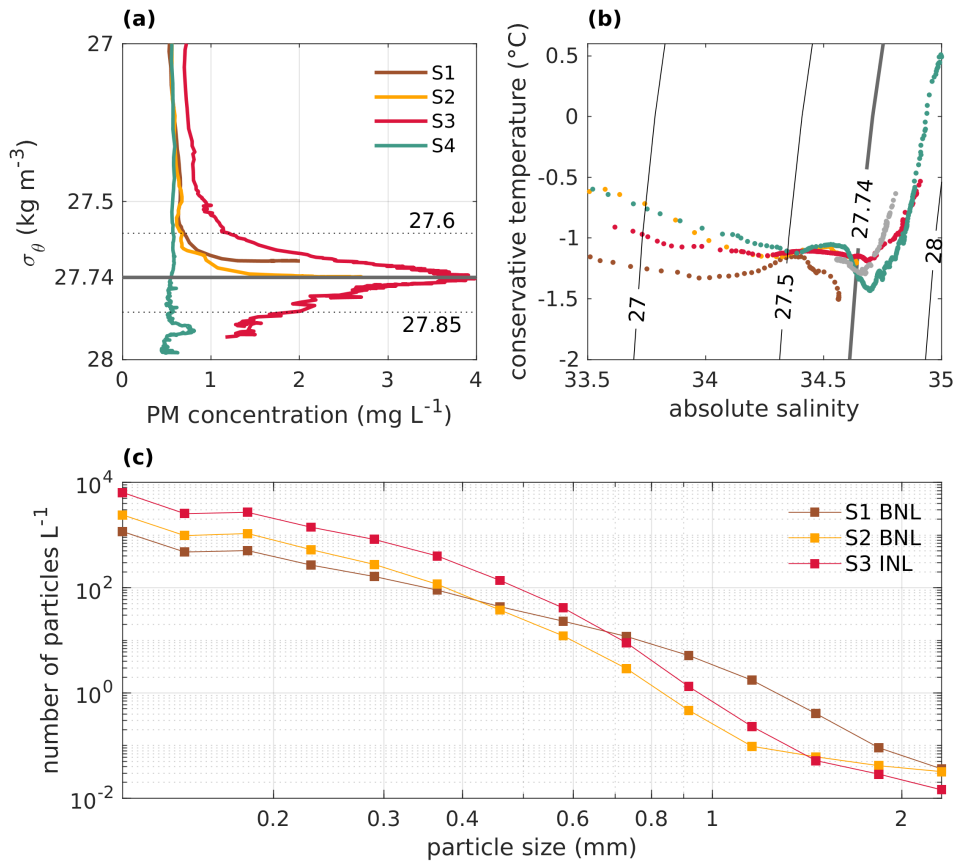


Figure 2. (a) Vertical profiles of PM concentration, displayed against density for stations S1–S4, and (b) the corresponding T-S diagrams. In (b), gray dots show a time series of the T-S data from the near-bottom moored CTD at M1 prior to recovery (second gray patch in Fig. 3). (c) Number of particles per particle size class at stations S1–S3, recorded with the UVP.

205 superimposed with weak ($\mathcal{O}(0.1) \text{ m s}^{-1}$), mainly barotropic semidiurnal tidal motions.
206 Current velocities are generally smaller and less variable between February and June,
207 compared to the time between July and January. While the transect profiles were mea-
208 sured, a period of intensified current velocities over the whole water column occurred,
209 with maximum depth-averaged velocities over 0.5 m s^{-1} , lasting for at least 24 hours (event
210 II, Fig. 3b). A similar event with intensified current velocities over a period of approx-
211 imately 48 hours was recorded 4 days earlier (event I, Fig. 3b). During both events, the
212 flow was mainly directed along-slope (eastward), but with a significant down-slope (north-
213 ward) component with a depth-averaged maximum current speed over 0.2 m s^{-1} . While
214 variations in sea surface height (black line, Fig. 3c) are mostly caused by tides (gray line,
215 Fig. 3c, tidal reconstruction based on the full three year time series, using the UTide Mat-
216 lab toolbox (Codiga, 2011)) and pressure data from the lowermost CTD, positive pres-
217 sure anomalies were recorded during both events.

218 Furthermore, a decrease of both water temperature and salinity, resulting in a de-
219 crease in potential density of over 0.2 kg m^{-3} within 24 hours indicates a strong down-
220 ward displacement of isopycnals (Fig. 3d). The corresponding vertical isopycnal displace-
221 ment was at least larger than the 100 m distance between the moored CTDs (see Fig. 3d).
222 The minimum density anomaly recorded during both events in the lowermost CTD, 27.7 kg m^{-3} ,
223 was found at a depth of approximately 70 m at the shelf station S2, suggesting that the
224 vertical displacement was probably even larger than 150 m.

225 The vertical structure of the time-averaged current profiles during the two events
226 (gray patches in Fig. 3) is very similar (Fig. 3e). Current velocities are vertically rather
227 homogeneous in the upper 80–140 m, around 0.3 m s^{-3} in eastward and 0.1 m s^{-1} in north-
228 ward (downslope) direction, and current velocities decrease towards the bottom. In par-
229 ticular, the eastward flow component exhibits strong shear in the deeper layers.

230 4 Discussion

231 4.1 Origin of the turbid layer

232 No similar INLs have been observed on the other ten transects measured during
233 the expedition, and hence no indication for the along-slope advection of material orig-
234 inating from upstream of the boundary current. The down-slope transport of PM in the
235 near bottom layer from the shallower continental shelf region as a dense gravity current,

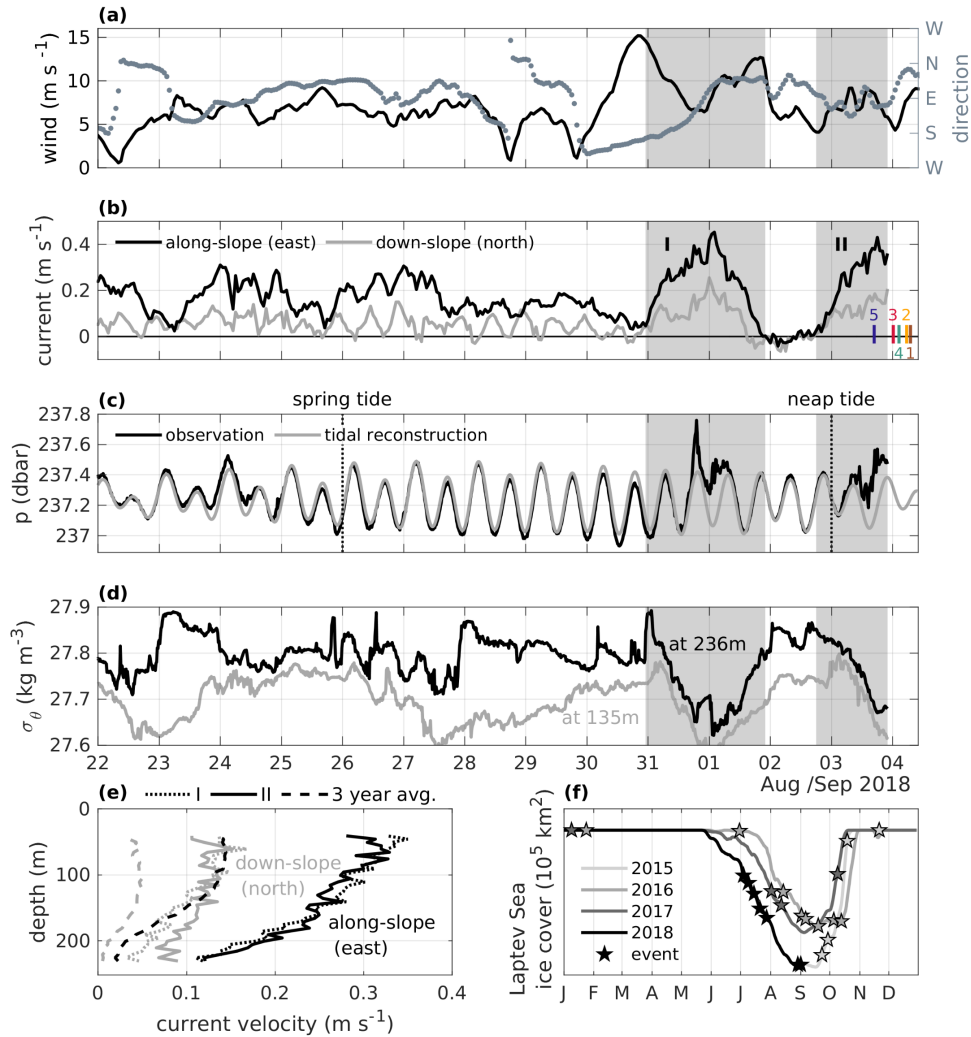


Figure 3. Time series of (a) wind speed (left vertical axis) and direction (right vertical axis), (b) depth-averaged current velocity in east (black line) and north (gray line) direction recorded with the moored ADCP at M1, (c) measured pressure (black line) and tidal reconstruction (gray line), and (d) density anomaly recorded with two CTDs at the M1 mooring (see Fig. 1). Colored lines in (b) indicate the time of the respective water column stations. (e) Vertical profiles of the current velocity in east (black lines) and north (gray line) direction, averaged over the duration of event I (dotted lines), event II (solid lines) and the 3 year deployment period (dashed lines). (f) Time series of Laptev Sea sea ice cover (km²), color-coded by year, with events (down-slope velocity >0.15 m s⁻¹, $\Delta\sigma_{\theta} >0.15$ kg m⁻³) indicated with stars.

236 and the subsequent detachment of this turbid layer near the shelf break, would result
237 in a cross-slope PM concentration gradient from high PM concentration at the upper shelf
238 to lower concentrations at the shelf break, opposite to the observed situation (Fig. 2a),
239 and is hence also unlikely. Furthermore, the strongly enhanced dissipation rates encoun-
240 tered at S3 point towards local resuspension, and a subsequent detachment and offslope
241 transport of the turbid near bottom layer. The similar PSD and water mass properties
242 in the INL at S3 and the BNL at S2 (Fig. 2c) further indicate that both turbid layers
243 have a common origin.

244 INLs are often characterized by uniform temperature and salinity properties (Thorpe
245 & White, 1988), which are associated with the water mass properties of the turbid near-
246 bottom layer from which they originate (Moum et al., 2002). While the density of the
247 turbid water mass observed over the slope is similar to the density of the near bottom
248 layer at the 94 m deep shelf station S2 (Fig. 2a), both the observed temperature and salin-
249 ity are slightly higher, by 0.04°C and 0.03, respectively, indicating that the observed in-
250 termediate PM concentration maximum originates from a slightly deeper position than
251 S2. Hence, the formation of the observed INL at S3 and the enhanced PM concentra-
252 tion in the near bottom layer at S2 can be conclusively explained by strong mixing and
253 local resuspension at the upper continental slope, and the subsequent detachment and
254 spreading of the turbid layer.

255 The question remains how the strong turbulence was generated. Frictional effects
256 alone are unlikely, as bottom boundary layers are typically confined to a few 10 m thick-
257 ness, and are characterized by suspended PM concentrations that increase towards the
258 bottom. A storm event with wind speeds up to 15 m s^{-1} and a change in wind direc-
259 tion from towards south-westerly to north-easterly directions took place on August 30,
260 but the winds decayed again shortly after (Fig. 3a). During the measurements, 4 days
261 later, winds were steady towards the north-east with speeds between $5\text{-}10\text{ m s}^{-1}$. How-
262 ever, wind-driven mixing is confined to the surface layer, even during a storm event, and
263 is unlikely to induce strongly enhanced dissipation at depths of over 300 m. Moreover,
264 local barotropic tidal currents and local tidal conversion (Rippeth et al., 2015) in this
265 region are weak.

266 We find the enhanced mid-water dissipation to coincide with a period of significant
267 down-slope barotropic flow and a depression in the isopycnals (Fig. 3b,d). In other con-

268 tinential slope regions in the Arctic, observed strong mid-water dissipation was found to
269 be associated with unsteady lee waves generated by a cross-isobath tidal current (Padman
270 et al., 1992; Rippeth et al., 2017; Fer et al., 2015, 2020). Based on an extensive obser-
271 vational data set including a 24 hour time series of temperature, salinity, dissipation rate
272 and current velocity profiles, Fer et al. (2020) report enhanced mid-water turbulence over
273 a period of 6 hours, following the downslope flow phase of a diurnal tidal current above
274 Yermak Plateau. The topographic setting (slope and water depth), and the magnitude
275 of the downslope velocity discussed here are comparable to the situation described in Fer
276 et al. (2020). Whilst in the case presented here the off-shelf barotropic flow is not the
277 result of a tide, which is weak in this region, the period of the downslope flow (~ 2 days,
278 see Fig. 3b) is longer than the local inertial period at this latitude, and so the lee wave
279 generated by the down-slope barotropic flow will be bottom trapped (Fer et al., 2015;
280 Rippeth et al., 2017). As such we identify the unsteady lee-wave mechanism, proposed
281 for dissipation of the tide over the shelf breaks poleward of the critical latitude (e.g. Rip-
282 peth et al., 2017; Fer et al., 2020), as potentially supporting the observed enhanced mid-
283 water dissipation.

284 4.2 Spatial and temporal distribution of INLs

285 Two events of enhanced (downslope) current velocities and downward isopycnal dis-
286 placement were recorded, 4 days before and during the measurements, and it is not im-
287 mediately clear which event lead to the formation of the observed INL. However, Fer et
288 al. (2020) found that bursts of high dissipation rates following a downward displacement
289 of isopycnals persisted only on time scales of hours. Furthermore, restratification after
290 the gravitational collapse of a mixed layer happens within hours (McPhee-Shaw, 2006),
291 and full restratification has not yet occurred at S3. It is hence likely that the second event
292 generated the observed strong mixing and consequently the INL above the upper slope.

293 The observed enhanced velocities might be linked to a larger scale continental shelf
294 wave, resulting from coastal convergences driven by cross-shelf Ekman transport, trig-
295 gered by the pan-Arctic wind field (Danielson et al., 2020). These waves are propagat-
296 ing eastward along the Arctic shelves, characterized by coastally enhanced sea level anoma-
297 lies and barotropic disturbances in the flow field, with largest current velocity anoma-
298 lies near the upper continental slope. The passage of a continental shelf wave and the
299 associated cross-slope barotropic pressure gradient would hence explain the observed en-

300 hanced current velocities in both east- and northward direction, but more observational
301 data are needed to confirm this hypothesis. Continental shelf waves were found to be episodic,
302 but re-occurring in the Arctic (Danielson et al., 2020). Based on a 9-year model hind-
303 cast, on average 12 surface anomalies linked to CSW were identified per year, with over
304 60 % of these anomalies occurring between August and January (Danielson et al., 2020).
305 This temporal distribution of CSWs roughly resembles the seasonal distribution of the
306 downslope flow events reported here (Fig. 3f), which occur exclusively between July and
307 January. Strong barotropic current surges of $0.4\text{--}0.5\text{ m s}^{-1}$, triggered by storms from
308 large scale pressure systems, were also found to cause frequently re-occurring sediment
309 resuspension at the upper slope (water depth of 140–150 m) of the Mackenzie shelf (Forest
310 et al., 2016).

311 Based on the three year mooring time series (summer 2015 to summer 2018), a to-
312 tal of 23 events with strong current velocity anomalies, a downward flow component $>$
313 0.15 m s^{-1} and a contemporaneous drop in potential density $>0.15\text{ kg m}^{-3}$ could be iden-
314 tified. These events occur mostly in the second half of the year, between July and Oc-
315 tober (Fig. 3f). Between February and June, no potential mixing events were recorded.
316 This seasonal distribution matches the uneven distribution of continental shelf waves found
317 in Danielson et al. (2020), which are a probable energy source for the enhanced turbu-
318 lent dissipation rates generating the INL. In addition, likelihood of INL formation varies
319 not only on seasonal, but also inter-annual scale. Both 2015 and 2018 were character-
320 ized by a long ice free season and a low minimum sea ice extent (Fig. 3f). For those years,
321 the mooring record covers only the freeze-up /melting season, respectively, but still a re-
322 latively high number of at least 4 /7 events were recorded. In 2016 and 2017, the annual
323 minimum Laptev Sea ice cover extent was larger compared to 2015 and 2018. Only 4 events
324 were recorded in 2017. In 2016 freeze-up was delayed by approximately two weeks (com-
325 pared to 2017), and 8 events were observed. The strong seasonality and interannual vari-
326 ability of potential mixing events towards periods with reduced ice cover in the Laptev
327 Sea suggests that INL formation is closely linked to the absence of sea ice. This supports
328 the hypothesis that their formation is linked to the presence of continental shelf waves.
329 A future reduction of the sea ice cover and elongated ice free periods may result in an
330 increasing number of INLs, and consequently significantly enhanced cross-shelf sediment
331 transport.

332 The absence of INLs on other transects might be a result of the episodic nature of
333 the flow anomalies that likely caused the INL formation, even though an INL might per-
334 sist for some time after the event, depending on the settling speed of the suspended par-
335 ticles. The spatially closest transect 125 km upstream of S3 was sampled on September
336 22. If an INL was formed there during the downslope flow event on September 3 (or a
337 later event), particles had already settled out. However, it is also conceivable that the
338 observed downslope flow at M2 is a spatially confined phenomenon, e.g. topographically
339 steered by an incision in the continental slope or a change in direction of the slope ori-
340 entation, and INLs are hence only generated over a limited along-slope distance. More
341 data is needed to assess both the duration and spatial distribution of INLs along the Laptev
342 Sea continental slope.

343 4.3 Cross-slope transport in the INL

344 We observed enhanced turbulent mixing which caused sediment resuspension and
345 a turbid layer characterized by a nearly uniform vertical distribution of temperature and
346 salinity, in line with previous INL observations at lower latitudes (e.g. Thorpe & White,
347 1988). The anticipated subsequent gravitational collapse of this layer will enhance hor-
348 izontal diffusivities, as the turbid layer spreads laterally along isopycnals (Thorpe & White,
349 1988; McPhee-Shaw et al., 2004; McPhee-Shaw, 2006). The lateral extent of an INL af-
350 ter the gravitational collapse is in theory bound by the internal Rossby radius $R = \frac{NH}{f}$,
351 where N is the buoyancy frequency, H the vertical length scale (here: 200 m) and f the
352 Coriolis frequency (McPhee-Shaw et al., 2004). Previously reported values for the lat-
353 eral extent of INLs are in the slightly larger (factor 1.4) than the internal Rossby radius
354 (16 km, continental slope off Porcupine Bank, NE Atlantic Thorpe & White, 1988), or
355 on the order of the internal Rossby radius (3-7 km, northern California margin McPhee-
356 Shaw et al., 2004; McPhee-Shaw, 2006). Depending on the varying background strat-
357 ification, the local Rossby radius in the Laptev Sea focus region ranges from 2.5-7.4 km.
358 Hence, particles transported within the observed INL over the steep slope ($\alpha = 0.15$) can
359 easily reach waters deeper than 1500 m. The distance between stations S3 and S4 ex-
360 ceeds the size of the local Rossby radius, which might explain the absence of an INL at
361 S4.

362 From the available data, it is impossible to assess the fraction of PM within the
363 INL that is ultimately exported to the deep basin. Considering 1 mg L^{-1} as a background

364 concentration (see S4, Fig. 1a), i.e. very fine material with a negligible settling velocity
365 that will not sink out, the integrated concentration of PM above background in the INL
366 at S3 is approximately 500 g m^{-2} . If only 1 % of this integrated concentration would
367 be transported towards the basin and subsequently settle at the sea floor, on average 8
368 INL events per year sum up to a total vertical PM flux of $40 \text{ g m}^{-2} \text{ y}^{-1}$. This value is
369 already higher than the estimated lateral input of lithogenic material to the surface sed-
370 iments off the Laptev Sea slope ($30 \text{ g m}^{-2} \text{ y}^{-1}$), reported by Fahl and Nöthig (2007) based
371 on sediment trap data from 1995/1996. This bias might indicate that the sedimentation
372 dynamics in the Laptev Sea continental slope region have substantially changed within
373 the last 20 years.

374 5 Conclusions

375 Observations from the Laptev Sea provide the first direct evidence of the existence
376 of turbid INLs over continental slopes both polewards of the critical M_2 latitude, and
377 in the Eurasian sector of the Arctic Ocean. The observed turbid layer likely originated
378 from the upper continental slope, at a water depth of 100–200 m. The cloud of PM ex-
379 tended over a vertical range from 60–310 m water depth and contained a total PM mass
380 of approximately 650 g m^{-2} and 10 g m^{-2} POC, which is potentially transported towards
381 deeper regions. Locally enhanced turbulent dissipation rates, inducing strong resuspen-
382 sion and vertical mixing, were probably caused by energy release from a trapped lee wave
383 initially developed by isopycnal displacement during intensified (down-slope) current ve-
384 locities associated with continental shelf waves. More focused observations, including high-
385 resolved time series of water column profiles, are needed to expose the link between con-
386 tinental shelf waves and enhanced mid-water dissipation.

387 Long-term current velocity data suggests that events potentially leading to an INL
388 formation are re-occurring and take place on average 8 times per year, almost exclusively
389 in the ice-free season (July to October), with strong inter-annual variability, probably
390 depending on the sea ice cover. Despite their relatively rare occurrence, INL formation
391 and the associated basin-ward transport of resuspended particles from the upper con-
392 tinental slope may substantially contribute to the cross-slope particle transport and the
393 vertical export of carbon in the Arctic Ocean.

394 The existence of INLs over the Laptev Sea continental slope emphasizes the close
395 connectivity between the Siberian shelves and the deep Arctic basins. In the future Arc-
396 tic, increasingly ice-free conditions may reinforce the cross-slope particle transport mech-
397 anism investigated in this study. In addition, local sediment supply from dirty sea ice
398 will increase with enhanced melting of first year ice in the marginal ice zone of the Siberian
399 Seas and central Arctic Ocean (Krumpfen et al., 2019). With increased shelf sea-ocean
400 coupling, pollutants introduced to the Arctic shelf seas (e.g. by increased marine traf-
401 fic and the offshore production of minerals and hydrocarbons) may affect the entire Arc-
402 tic ecosystem. The discovery of an intermittent off-shelf transport mechanism linked to
403 enhanced turbulent mixing and apparently associated with continental shelf waves is clearly
404 an area requiring further study, particularly as it implies cross-slope particle transport
405 will likely increase with declining sea ice cover.

406 **Acknowledgments**

407 We would like to thank the crew and participants of the Akademik Tryoshnikov cruise,
408 Igor Polyakov and Ben Möller. Financial support was received from the German Fed-
409 eral Ministry for Science and Education (BMBF) as part of the Changing Arctic Trans-
410 polar System (CATS, grant number 03F0776), as well as for the NERC-BMBF-funded
411 PEANUTS-project (grant number 03F0804A and NE/R01275X/1).

412 Fig. 1a was produced using the `m_map` matlab toolbox (Pawlowicz, 2000).

413 Fig. 3a shows wind data from ECMWF Reanalysis v5 (ERA5), produced by the
414 Copernicus Climate Change Service (C3S). Sea ice data displayed in Fig. 3f is available
415 at: Fetterer, F., K. Knowles, W. N. Meier, M. Savoie, and A. K. Windnagel. 2017, up-
416 dated daily. Sea Ice Index, Version 3. [G02135, Laptev Sea]. Boulder, Colorado USA.
417 NSIDC: National Snow and Ice Data Center. doi: <https://doi.org/10.7265/N5K072F8>.
418 Date Accessed: March 15, 2021.

419 Hydrographic data used in this study were obtained under the framework of the
420 NABOS project with support from NSF (Grants AON-1203473 and AON-1947162), and
421 are available at:

422 Igor Polyakov. 2019. Acoustic Doppler Current Profiler (ADCP) from moorings taken
423 in the Eurasian and Makarov basins, Arctic Ocean, 2015-2018. Arctic Data Center. doi:10.18739/A2HT2GB80;

424 Igor Polyakov and Robert Rember. 2019. Conductivity, Temperature, Pressure (CTD)
425 measurements from Sea Bird Electronics SBE37 instruments taken in the Eurasian and
426 Makarov basins, Arctic Ocean, 2015-2018. Arctic Data Center. doi:10.18739/A2NK3652R;

427 Janout, Markus A; Tippenhauer, Sandra; Schulz, Kirstin; Mohrholz, Volker; Ivanov,
428 Vladimir; Polyakov, Igor (2020): Microstructure measurements during Akademik Tryosh-
429 nikov cruise AT2018 to the Arctic Ocean. PANGAEA, <https://doi.pangaea.de/10.1594/PANGAEA.925880>.

430 References

431 Azetsu-Scott, K., Johnson, B. D., & Petrie, B. (1995). An intermittent, intermedi-
432 ate nepheloid layer in Emerald Basin, Scotian shelf. *Continental shelf research*,
433 *15*(2-3), 281–293. doi: [https://doi.org/10.1016/0278-4343\(93\)E0003-Q](https://doi.org/10.1016/0278-4343(93)E0003-Q)

434 Boetius, A., Albrecht, S., Bakker, K., Bienhold, C., Felden, J., Fernández-Méndez,
435 M., ... others (2013). Export of algal biomass from the melting arctic sea ice.
436 *Science*, *339*(6126), 1430–1432. doi: 10.1126/science.1231346

437 Cacchione, D., & Drake, D. (1986). Nepheloid layers and internal waves over conti-
438 nental shelves and slopes. *Geo-Marine Letters*, *6*(3), 147–152. doi: <https://doi.org/10.1007/BF02238085>

440 Codiga, D. L. (2011). Unified tidal analysis and prediction using the UTide Matlab
441 functions.

442 Danielson, S. L., Hennon, T. D., Hedstrom, K. S., Pnyushkov, A. V., Polyakov,
443 I. V., Carmack, E., ... others (2020). Oceanic routing of wind-sourced energy
444 along the Arctic continental shelves. *Frontiers in Marine Science*, *7*, 509. doi:
445 <https://doi.org/10.3389/fmars.2020.00509>

446 de Madron, X. D., Castaing, P., Nyffeler, F., & Courp, T. (1999). Slope transport
447 of suspended particulate matter on the Aquitanian margin of the Bay of Bis-
448 cay. *Deep Sea Research Part II: Topical Studies in Oceanography*, *46*(10),
449 2003–2027. doi: [https://doi.org/10.1016/S0967-0645\(99\)00053-3](https://doi.org/10.1016/S0967-0645(99)00053-3)

450 De Madron, X. D., Nyffeler, F., & Godet, C. H. (1990). Hydrographic structure and
451 nepheloid spatial distribution in the Gulf of Lions continental margin. *Conti-
452 nental Shelf Research*, *10*(9-11), 915–929. doi: [https://doi.org/10.1016/0278-4343\(90\)90067-V](https://doi.org/10.1016/0278-4343(90)90067-V)

454 Dickson, R., & McCave, I. (1986). Nepheloid layers on the continental slope west of
455 Porcupine Bank. *Deep Sea Research Part A. Oceanographic Research Papers*,

456 33(6), 791–818. doi: [https://doi.org/10.1016/0198-0149\(86\)90089-0](https://doi.org/10.1016/0198-0149(86)90089-0)

457 Fahl, K., & Nöthig, E.-M. (2007). Lithogenic and biogenic particle fluxes on the
458 Lomonosov Ridge (central Arctic Ocean) and their relevance for sediment ac-
459 cumulation: Vertical vs. lateral transport. *Deep Sea Research Part I: Oceanographic Research Papers*, 54(8), 1256–1272. doi: [https://doi.org/10.1016/](https://doi.org/10.1016/j.dsr.2007.04.014)
460 [j.dsr.2007.04.014](https://doi.org/10.1016/j.dsr.2007.04.014)

462 Fer, I., Koenig, Z., Kozlov, I. E., Ostrowski, M., Rippeth, T. P., Padman, L., ...
463 Kolås, E. (2020). Tidally Forced Lee Waves Drive Turbulent Mixing Along the
464 Arctic Ocean Margins. *Geophysical Research Letters*, 47(16), e2020GL088083.
465 doi: <https://doi.org/10.1029/2020GL088083>

466 Fer, I., Müller, M., & Peterson, A. (2015). Tidal forcing, energetics, and mixing
467 near the Yermak Plateau. *Ocean Sci*, 11, 287–304. doi: [doi:10.5194/os-11-287](https://doi.org/10.5194/os-11-287-2015)
468 -2015

469 Forest, A., Osborne, P. D., Curtiss, G., & Lowings, M. G. (2016). Current surges
470 and seabed erosion near the shelf break in the Canadian Beaufort Sea: A re-
471 sponse to wind and ice motion stress. *Journal of Marine Systems*, 160, 1–16.
472 doi: <https://doi.org/10.1016/j.jmarsys.2016.03.008>

473 Forest, A., Osborne, P. D., Fortier, L., Sampei, M., & Lowings, M. G. (2015).
474 Physical forcings and intense shelf-slope fluxes of particulate matter in the
475 halocline waters of the Canadian Beaufort Sea during winter. *Continental Shelf*
476 *Research*, 101, 1–21. doi: <https://doi.org/10.1016/j.csr.2015.03.009>

477 Forest, A., Sampei, M., Hattori, H., Makabe, R., Sasaki, H., Fukuchi, M., ...
478 Fortier, L. (2007). Particulate organic carbon fluxes on the slope of
479 the Mackenzie Shelf (Beaufort Sea): Physical and biological forcing of
480 shelf-basin exchanges. *Journal of Marine Systems*, 68(1-2), 39–54. doi:
481 <https://doi.org/10.1016/j.jmarsys.2006.10.008>

482 Gardner, W. D., & Walsh, I. D. (1990). Distribution of macroaggregates and fine-
483 grained particles across a continental margin and their potential role in fluxes.
484 *Deep Sea Research Part A. Oceanographic Research Papers*, 37(3), 401–411.
485 doi: [https://doi.org/10.1016/0198-0149\(90\)90016-O](https://doi.org/10.1016/0198-0149(90)90016-O)

486 Gorsky, G., Ohman, M. D., Picheral, M., Gasparini, S., Stemmann, L., Romagnan,
487 J.-B., ... Prejger, F. (2010). Digital zooplankton image analysis using the
488 ZooScan integrated system. *Journal of plankton research*, 32(3), 285–303. doi:

489 <https://doi.org/10.1093/plankt/fbp124>

490 Honjo, S., Krishfield, R. A., Eglinton, T. I., Manganini, S. J., Kemp, J. N., Do-
491 herty, K., . . . Takizawa, T. (2010). Biological pump processes in the cry-
492 opelagic and hemipelagic Arctic Ocean: Canada Basin and Chukchi Rise.
493 *Progress in Oceanography*, 85(3-4), 137–170. doi: [https://doi.org/10.1016/](https://doi.org/10.1016/j.pocean.2010.02.009)
494 [j.pocean.2010.02.009](https://doi.org/10.1016/j.pocean.2010.02.009)

495 Hwang, J., Eglinton, T. I., Krishfield, R. A., Manganini, S. J., & Honjo, S. (2008).
496 Lateral organic carbon supply to the deep Canada Basin. *Geophysical Research*
497 *Letters*, 35(11). doi: <https://doi.org/10.1029/2008GL034271>

498 Hwang, J., Kim, M., Manganini, S. J., McIntyre, C. P., Haghypour, N., Park, J., . . .
499 Eglinton, T. I. (2015). Temporal and spatial variability of particle transport
500 in the deep Arctic Canada Basin. *Journal of Geophysical Research: Oceans*,
501 120(4), 2784–2799. doi: <https://doi.org/10.1002/2014JC010643>

502 Krumpfen, T., Belter, H. J., Boetius, A., Damm, E., Haas, C., Hendricks, S., . . .
503 others (2019). Arctic warming interrupts the transpolar drift and affects long-
504 range transport of sea ice and ice-rafted matter. *Scientific reports*, 9(1), 1–9.
505 doi: <https://doi.org/10.1038/s41598-019-41456-y>

506 McCave, I., & Hall, I. R. (2002). Turbidity of waters over the Northwest Iberian
507 continental margin. *Progress in Oceanography*, 52(2-4), 299–313. doi: [https://](https://doi.org/10.1016/S0079-6611(02)00012-5)
508 [doi.org/10.1016/S0079-6611\(02\)00012-5](https://doi.org/10.1016/S0079-6611(02)00012-5)

509 McPhee-Shaw, E. (2006). Boundary–interior exchange: reviewing the idea that
510 internal-wave mixing enhances lateral dispersal near continental margins. *Deep*
511 *Sea Research Part II: Topical Studies in Oceanography*, 53(1-2), 42–59. doi:
512 <https://doi.org/10.1016/j.dsr2.2005.10.018>

513 McPhee-Shaw, E., Sternberg, R., Mullenbach, B., & Ogston, A. (2004). Ob-
514 servations of intermediate nepheloid layers on the northern California
515 continental margin. *Continental Shelf Research*, 24(6), 693–720. doi:
516 <https://doi.org/10.1016/j.csr.2004.01.004>

517 Moum, J., Caldwell, D., Nash, J., & Gunderson, G. (2002). Observations of bound-
518 ary mixing over the continental slope. *Journal of Physical Oceanography*,
519 32(7), 2113–2130. doi: [https://doi.org/10.1175/1520-0485\(2002\)032<2113:](https://doi.org/10.1175/1520-0485(2002)032<2113:OOBMOT>2.0.CO;2)
520 [OOBMOT>2.0.CO;2](https://doi.org/10.1175/1520-0485(2002)032<2113:OOBMOT>2.0.CO;2)

521 OBrien, M., Macdonald, R., Melling, H., & Iseki, K. (2006). Particle fluxes and

- 522 geochemistry on the Canadian Beaufort Shelf: Implications for sediment
523 transport and deposition. *Continental Shelf Research*, 26(1), 41–81. doi:
524 <https://doi.org/10.1016/j.csr.2005.09.007>
- 525 Osborne, P. D., & Forest, A. (2016). Sediment Dynamics from Coast to Slope–
526 Southern Canadian Beaufort Sea. *Journal of Coastal Research*(75), 537–541.
527 doi: <https://doi.org/10.2112/SI75-108.1>
- 528 Padman, L., Plueddemann, A. J., Muench, R. D., & Pinkel, R. (1992). Diurnal tides
529 near the Yermak Plateau. *Journal of Geophysical Research: Oceans*, 97(C8),
530 12639–12652. doi: <https://doi.org/10.1029/92JC01097>
- 531 Pak, H., Zaneveld, J. R. V., & Kitchen, J. (1980). Intermediate nepheloid layers ob-
532 served off Oregon and Washington. *Journal of Geophysical Research: Oceans*,
533 85(C11), 6697–6708. doi: <https://doi.org/10.1029/JC085iC11p06697>
- 534 Pawlowicz, R. (2000). M_Map: A mapping package for Matlab. *Univer-*
535 *sity of British Columbia Earth and Ocean Sciences*. [Online]. Available:
536 <http://www.eos.ubc.ca/rich/map.html>.
- 537 Polyakov, I. V., Rippeth, T. P., Fer, I., Alkire, M. B., Baumann, T. M., Carmack,
538 E. C., ... others (2020). Weakening of cold halocline layer exposes sea ice
539 to oceanic heat in the eastern Arctic Ocean. *Journal of Climate*, 33(18),
540 8107–8123. doi: <https://doi.org/10.1175/JCLI-D-19-0976.1>
- 541 Polyakov, I. V., Rippeth, T. P., Fer, I., Baumann, T. M., Carmack, E. C., Ivanov,
542 V. V., ... Rember, R. (2020). Intensification of Near-Surface Currents and
543 Shear in the Eastern Arctic Ocean. *Geophysical Research Letters*, 47(16),
544 e2020GL089469. doi: <https://doi.org/10.1029/2020GL089469>
- 545 Puig, P., Company, J. B., Sardà, F., & Palanques, A. (2001). Responses of
546 deep-water shrimp populations to intermediate nepheloid layer detach-
547 ments on the Northwestern Mediterranean continental margin. *Deep Sea*
548 *Research Part I: Oceanographic Research Papers*, 48(10), 2195–2207. doi:
549 [https://doi.org/10.1016/S0967-0637\(01\)00016-4](https://doi.org/10.1016/S0967-0637(01)00016-4)
- 550 Puig, P., & Palanques, A. (1998). Nepheloid structure and hydrographic control on
551 the Barcelona continental margin, northwestern Mediterranean. *Marine Geol-*
552 *ogy*, 149(1-4), 39–54. doi: [https://doi.org/10.1016/S0025-3227\(98\)00037-1](https://doi.org/10.1016/S0025-3227(98)00037-1)
- 553 Rippeth, T. P., Lincoln, B. J., Lenn, Y.-D., Green, J. M., Sundfjord, A., & Ba-
554 con, S. (2015). Tide-mediated warming of Arctic halocline by Atlantic

- 555 heat fluxes over rough topography. *Nature Geoscience*, 8(3), 191. doi:
556 <https://doi.org/10.1038/ngeo2350>
- 557 Rippeth, T. P., Vlasenko, V., Stashchuk, N., Scannell, B. D., Green, J. M., Lincoln,
558 B. J., & Bacon, S. (2017). Tidal conversion and mixing poleward of the critical
559 latitude (an Arctic case study). *Geophysical Research Letters*, 44(24), 12–349.
560 doi: <https://doi.org/10.1002/2017GL075310>
- 561 Schulz, K., Endoh, T., & Umlauf, L. (2017). Slope-induced tidal straining: Analysis
562 of rotational effects. *Journal of Geophysical Research: Oceans*, 122(3), 2069–
563 2089. doi: <https://doi.org/10.1002/2016JC012448>
- 564 Schulz, K., Janout, M., Lenn, Y.-D., Ruiz-Castillo, E., Polyakov, I., Mohrholz, V.,
565 ... Vredenburg, M. (2021). On the along-slope heat loss of the Boundary Cur-
566 rent in the Eastern Arctic Ocean. *Journal of Geophysical Research: Oceans*,
567 126(2), e2020JC016375. doi: <https://doi.org/10.1029/2020JC016375>
- 568 Schulz, K., & Umlauf, L. (2016). Residual transport of suspended material by tidal
569 straining near sloping topography. *Journal of Physical Oceanography*, 46(7),
570 2083–2102. doi: <https://doi.org/10.1175/JPO-D-15-0218.1>
- 571 Sprent, P. (2012). *Applied nonparametric statistical methods*. Springer Science &
572 Business Media.
- 573 Tarasenko, A., Supply, A., Kusse-Tiuz, N., Ivanov, V., Makhotin, M., Tournadre,
574 J., ... Kolodziejczyk, N. (2021). Surface waters properties in the Laptev and
575 the East-Siberian Seas in summer 2018 from in situ and satellite data. *Ocean
576 Science*, 17(1), 221–247. doi: <https://doi.org/10.5194/os-17-221-2021>
- 577 Thorpe, S., & White, M. (1988). A deep intermediate nepheloid layer. *Deep
578 Sea Research Part A. Oceanographic Research Papers*, 35(9), 1665–1671. doi:
579 [https://doi.org/10.1016/0198-0149\(88\)90109-4](https://doi.org/10.1016/0198-0149(88)90109-4)
- 580 van Weering, T. C., De Stigter, H. C., Balzer, W., Epping, E. H., Graf, G., Hall,
581 I. R., ... others (2001). Benthic dynamics and carbon fluxes on the NW
582 European continental margin. *Deep Sea Research Part II: Topical Stud-
583 ies in Oceanography*, 48(14-15), 3191–3221. doi: [https://doi.org/10.1016/
584 S0967-0645\(01\)00037-6](https://doi.org/10.1016/S0967-0645(01)00037-6)
- 585 Wegner, C., Hoesemann, J. A., Dmitrenko, I., Kirillov, S., Tuschling, K., Abramova,
586 E., & Kassens, H. (2003). Suspended particulate matter on the Laptev Sea
587 shelf (Siberian Arctic) during ice-free conditions. *Estuarine, Coastal and Shelf*

588 *Science*, 57(1-2), 55–64. doi: [https://doi.org/10.1016/S0272-7714\(02\)00328-1](https://doi.org/10.1016/S0272-7714(02)00328-1)
589 Xiang, Y., & Lam, P. J. (2020). Size-Fractionated Compositions of Marine Sus-
590 pended Particles in the Western Arctic Ocean: Lateral and Vertical Sources.
591 *Journal of Geophysical Research: Oceans*, 125(8), e2020JC016144. doi:
592 <https://doi.org/10.1029/2020JC016144>

Accepted Article